Acoustic behaviors of the microperforated panel absorber array in nonlinear regime under moderate acoustic pressure excitation

Y. K. Chiang and Y. S. Choy

ARTICLES YOU MAY BE INTERESTED IN

Acoustic behaviors of the microperforated panel absorber array in nonlinear regime under moderate acoustic pressure excitation

Y. K. Chiang and Y. S. Choy[a)]

*Department of Mechanical Engineering, The Hong Kong Polytechnic University, Hung Hom, Kowloon,
Hong Kong Special Administrative Region, China*

The acoustic performance of a microperforated panel (MPP) absorber array in the nonlinear regime is investigated both numerically and experimentally. The MPP absorber array is constructed by three parallel-arranged MPP absorbers with different cavity depths. A finite element model is used to simulate the acoustic response of the MPP absorber array by adopting the nonlinear impedance model. The results show that the absorption of the MPP absorber array is affected by the incident sound pressure when it is beyond around 100 dB. With appropriate structural and perforation property of MPP, the MPP absorber array in non-linear regime outperforms that in linear regime due to the improvement of equivalent acoustic impedance matching with ambient air over wide frequency range. However, when the sound pressure excitation is too high, the local resonance effect of the resonating component MPP absorber is diminished and the sound absorption is decreased. With the carefully chosen properties of MPP, the performance degradation induced by panel vibration can be avoided. An optimal set of MPP properties to avoid the performance degradation induced by panel vibration is determined. The measured normal absorption coefficients of a prototype MPP absorber array compare well with the numerical prediction in both linear and nonlinear regimes.
© 2018 Acoustical Society of America. https://doi.org/10.1121/1.5021334

I. INTRODUCTION

In recent decades, numerous studies about the sound absorption performance of the different absorbers have been carried out. The traditional dissipative approach with fibrous material (Ingard, 1994) can provide desirable absorption at mid to high frequencies, but the sound absorption is insufficient at low frequencies due to a strong impedance mismatch. In order to reduce the large surface impedance of a conventional absorber, microperforated panel (MPP) absorber has been proposed by Maa (1975) as a promising fiber-free alternative to the porous materials for broadband noise control. MPPs are thin panels with numerous orifices of diameter in sub-millimeter scale. The small perforations provide sufficient acoustic resistance and low acoustic reactance for sound absorption. Based on the theory and the empirical impedance model of MPP introduced by Maa (1998), the acoustic performance of such device can be predicted in the linear regime. The absorption properties of the microperforations can improve the performance of the plate silencer with a wider stopband (Wang *et al.*, 2012). However, in many circumstances, the MPP absorber is exposed to extreme environments at high sound pressure level such as aircraft engines and mass production machinery in factory. A number of researchers have studied the acoustic behaviors of the orifice when it is subjected to high sound intensity (Sivian, 1935; Thurston *et al.*, 1957). From the flow visualizations, Salikuddin and Ahuja (1983) observed the flow separation and the jet formation at the exit

of orifice. The acoustic energy is converted to the vortical energy due to the vortex ring formation. Such acoustic nonlinearity of the orifice changes the acoustic performance of the MPP.

Several studies were conducted to investigate the nonlinear effects on the acoustic impedance of the orifice (Ingard and Labate, 1950). Ingard and Ising (1967) studied the nonlinear behavior of acoustic impedance of an orifice in the absence of mean fluid flow by measuring the air particle velocity in the orifice and the acoustic pressure fluctuations producing the flow simultaneously. They showed that the acoustic resistance increases proportionally with the flow velocity in the orifice, and the acoustic reactance decreases at high sound pressure. Cummings and Eversman (1983) established a simple quasi-steady model by introducing the empirical vena contracta coefficient to explain the acoustic energy dissipation mechanism. Cummings (1986) developed the numerical time-domain (NTD) model to examine the acoustic power losses induced by the production of vorticity at the orifice lip in the presence of high-amplitude sound wave. The equation of motion for the air is numerically integrated in time domain, and hence, the details of the pressure-time history of the wave transmitted through the orifice can be predicted. Hersh *et al.* (2003) further developed the quasi-steady model with the use of discharge coefficient as the nonlinear parameter to predict the nonlinear acoustic impedance for both single and multiple orifices over a wide range of sound pressure levels and frequencies. Instead of using the quasi-steady model with the empirical parameter, Maa (1996) suggested a nonlinear acoustic impedance which is a combination of the linear impedance and the end

[a)]Electronic mail: mmyschoy@polyu.edu.hk

correction which is directly related to the air particle velocity in the orifice. Tayong *et al.* (2010) proposed another nonlinear impedance model in terms of the Mach number in the perforation based on the dimensional analysis and Forchheimer's law in order to study the acoustic behavior of the MPP absorber at high sound excitation. Park (2013) introduced an empirical nonlinear impedance model which considers all geometric parameters of the MPP and the incident pressure. He calculated the flow velocity in the orifice from the incident pressure by using the Bernoulli's law and the acoustic circuit analogy. The results showed that a better sound absorption can be achieved by the single MPP absorber at high sound pressure level with the same parameters of MPP.

Although the MPP absorber performs well with high absorption at its resonance frequency, its effective frequency band is insufficient to compete with the porous materials. In order to further extend the absorption bandwidth, double-layer (Zhang and Gu, 1998) or even multiple-layer MPP absorbers (Lee and Kwon, 2004; Mu *et al.*, 2011) are suggested. The sound absorption behaviors of the double-layer MPP absorber (or double-leaf MPP absorber) were investigated theoretically under the normal incidence excitation (Sakagami *et al.*, 2006). The absorption mechanism of the double-layer MPP absorber was found to be a combination of resonator type absorption at mid-to-high frequencies and acoustic flow resistance at low frequency. Hence, comparing with the traditional single MPP absorber, a considerable supplementary absorption can be obtained at low frequency. The absorption performance over broadband frequency range can be further improved by increasing the number of MPPs. However, the size of multiple-layer MPP absorber would increase with the number of layers, and hence, extra space is required. Recently, some researchers introduced another more straightforward approach by combining multiple MPP absorbers with different frequency characteristics in parallel for broadband performance. Zha *et al.* (1994) studied the normal incidence absorption performance of the MPP absorber array with two sub-cavities based on Maa's impedance model in the linear regime. The absorption coefficients of the MPP absorber array were measured experimentally by using the impedance tube. Wang and Huang (2011) later established a finite element model to simulate the acoustic behaviors of the parallel arrangement of three MPP absorbers with different cavity depths at normal incidence. The numerical results showed that a broader absorption bandwidth can be achieved by the device based on the parallel absorption mechanism. The absorption performances of the same configuration with three sub-cavities which are partially filled with different types of polymer materials were also investigated numerically and experimentally (Wang and Choy, 2015). Recently, Wang *et al.* (2014) established a three-dimensional finite element model to study the effect of different angle of incidence wave on the MPP absorber array which consists of four sub-cavities. Most of existing works focused on the absorption characteristics of the MPP absorber arrays in the linear regime. However, the MPP absorbers would be adopted in the environment with moderate or high sound pressure excitation. At the moderate sound pressure level, at which the acoustic field is linear, the local nonlinearity of orifice would be induced by the acoustic excitation. Few efforts have been made to study the acoustic response of the MPP absorber array with the effect of local nonlinearity of orifice. Also, the acoustic performance of the MPP absorber array subjected to moderate acoustic excitation has not been studied. The purpose of this study is to investigate the acoustic behaviors of the MPP absorber array under moderate acoustic excitation, at which the acoustic field is maintained as linear. It is different from the previous studies which mainly focused on the acoustic behaviors of MPP absorber in the linear regime. Moreover, this study is distinct from the literature about the nonlinear effect of orifice which only studied the performance of single MPP absorber. The present study focuses on the investigation of the effect of local nonlinearity of orifice on the acoustic response of MPP absorber array with different sub-cavity configuration.

In what follows, Sec. II outlines the two-dimensional finite element modelling of the MPP absorber array. Section III shows the numerical predictions of the absorption performance and the acoustic behaviors of the MPP absorber array in the nonlinear regime. Section IV describes the experimental measurements for the model validation. The main conclusions are summarized in Sec. V.

II. FINITE ELEMENT MODELING

A finite element model is established based on a two-dimensional configuration of the rectangular MPP absorber array. Figure 1 shows one basic module of the MPP absorber array which is adopted in the present study. The MPP is backed by three rectangular sub-cavities with different cavity depths D_1, D_2, and D_3. The walls of the duct and sub-cavities as well as the partitions are regarded as acoustically rigid. The MPP itself can be either rigid or flexible which depends on the material of the panel. The normal incident sound p_i is assumed as a plane wave. When the acoustic wave is incident on the MPP, part of the sound energy is reflected, while the rest is dissipated by the MPP. The reflected sound wave is represent by p_r. The height of the duct is denoted by h in the foregoing sections as shown in Fig. 1.

The finite element procedure is established to simulate the acoustic behaviors of the MPP absorber array with the local nonlinearity features of the perforations induced by moderate acoustic excitation. The finite element model consists of two acoustic domains and one structural domain
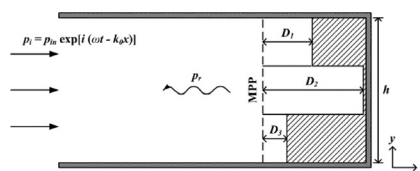

FIG. 1. Schematic diagram of the MPP absorber array with three partitioned sub-cavities.

J. Acoust. Soc. Am. **143** (1), January 2018

Y. K. Chiang and Y. S. Choy   539

which are the duct, backing sub-cavities and the MPP, respectively. In the current study, the effect of the orifice local nonlinearity on the absorption performance of the MPP absorber array is investigated under the acoustic pressure excitation range from 50 to 120 dB. At sound pressure level (SPL) = 120 dB, the air particle velocity is 0.0679 m/s, and hence the acoustic Mach number Ma is low, i.e., Ma is the ratio of the air particle velocity to the sound speed, which is only 2×10^{-4}. For low acoustic Mach number, i.e., $Ma \ll 1$, the acoustic field can be regarded as linear acoustics (Crocker, 1998). Thus, the sound field inside the duct and backing sub-cavities are governed by the Helmholtz equation

$$(\nabla^2 + k_0^2)\phi = 0, \tag{1}$$

where $k_0 = \omega/c_0$ is the wavenumber, c_0 is the sound speed, $\omega = 2\pi f$ denotes the angular frequency, and ϕ is the velocity potential. The acoustic pressure p and the particle velocity u can by expressed by the velocity potential,

$$p = -i\omega\rho_0\phi, \quad u = \nabla\phi, \tag{2}$$

where i is the imaginary unit and ρ_0 is the density of air. The plane sound wave is incident on the MPP from the left hand side of the duct,

$$p_i = p_{in} \exp[i(\omega\tau - k_0x)], \tag{3}$$

where p_{in} is the amplitude of incident sound wave. The effect of the MPP is implemented as the equivalent acoustic impedance. By neglecting the vibration of the panel, the boundary condition at the interface of the rigid MPP is formulated as

$$\left.\frac{\partial\phi}{\partial x}\right|_{rigid} = \frac{p_{cav} - p_{duct}}{\rho_0 c_0 Z}, \tag{4}$$

where p_{duct} and p_{cav} represent the acoustic pressure on the duct side and the backing cavity side, respectively, and Z is the specific acoustic impedance of the MPP. It can be written as

$$Z = Z_{resist} + Z_{react}, \tag{5}$$

where Z_{resist} is the specific acoustic resistance and Z_{react} is the acoustic reactance. As stated by Maa (1998) and Park (2013), each term for linear and nonlinear can be expressed as

$$Z_{resist} = \begin{cases} \dfrac{32vt}{\sigma\rho_0c_0d^2}\left[\left(1+\dfrac{K^2}{32}\right)^{1/2} + \dfrac{\sqrt{2}}{8}K\dfrac{d}{t}\right], & \text{for linear case,} \\[4mm] \dfrac{32vt}{\sigma\rho_0c_0d^2}\left[\left(1+\dfrac{K^2}{32}\right)^{1/2} + \dfrac{\sqrt{2}}{8}K\dfrac{d}{t}\right] + 1.59\left(\dfrac{d}{t}\right)^{0.06}\sigma^{-0.845}\left[\sigma\left(\sqrt{0.25+\dfrac{2p_{in}}{\rho_0c_0^2\sigma^2}} - 0.5\right)\right], & \text{for nonlinear case,} \end{cases} \tag{6a}$$

$$Z_{react} = \begin{cases} \dfrac{i\omega t}{\sigma c_0}\left[1+\left(9+\dfrac{K^2}{2}\right)^{-1/2} + 0.85\dfrac{d}{t}\right], & \text{for linear case,} \\[4mm] \dfrac{i\omega t}{\sigma c_0}\left[1+\left(9+\dfrac{K^2}{2}\right)^{-1/2} + 0.85\dfrac{d}{t}\left(1+\dfrac{1}{1-\sigma^2}\left(\sqrt{0.25+\dfrac{2p_{in}}{\rho_0c_0^2}\times\dfrac{1-\sigma^2}{\sigma^2}} - 0.5\right)\right)^{-1}\right], & \text{for nonlinear case,} \end{cases} \tag{6b}$$

where $K = d\sqrt{\omega\rho_0/4v}$, v denotes the coefficient of dynamic viscosity of air, d is the orifice diameter, t is the thickness of MPP, and σ is the perforation ratio.

When the acoustic excitation increases and a light panel is used, the effects of the structural vibration of the perforated panel on the acoustic performance can be significant at the resonance frequency of the MPP. The vibration of the perforated panel is coupled with the acoustic fields on the duct and backing cavity sides. The motion of the perforated panel is governed by the following equation:

$$B\nabla^4\eta(y,t) - \omega^2M\eta(y,t) = p_{duct} - p_{cav}, \quad 0 < y < h, \qquad \begin{cases} \eta = 0, \dfrac{\partial\eta}{\partial y} = 0, & \text{fixed edges,} \\[3mm] \eta = 0, \dfrac{\partial^2\eta}{\partial y^2} = 0, & \text{pinned edges,} \end{cases} \tag{7}$$

where η denotes the normal displacement of panel, h is the height of MPP absorber, B is the bending stiffness of the plate, and M is the MPP surface density which is defined as the plate mass per unit surface area. It is assumed that the panel vibration amplitude is small, and thus the elastic material behavior of the panel is not considered in the present

study. The edges of the MPP can be either fixed or pinned. For a vibro-acoustic coupling model, another boundary condition at the interface between the flexible perforated panel and the acoustic domains is needed to replace that of the rigid panel which is shown in Eq. (4). When the perforated panel vibrates, the viscous force at the air–solid interface in

Y. K. Chiang and Y. S. Choy

the orifice depends on the relative velocity between the normal vibration velocity of the panel $u_p = i\omega\eta$ and the air particle velocity inside the orifice. Thus, the boundary conditions of the flexible MPP becomes (Takahashi and Tanaka, 2002)

$$\left.\frac{\partial\phi}{\partial x}\right|_{flexible} = \left(1 - \frac{\sigma Z_{react}}{Z}\right)u_p + \frac{p_{cav} - p_{duct}}{\rho_0 c_0 Z}. \quad (8)$$

At the inlet of the duct, the Dirichlet-to-Neumann (DtN) boundary condition is applied to describe the no-reflection condition. The detail expression of the DtN boundary condition have been given by Wang and Huang (2011). The duct walls and the partitions are treated as acoustically rigid, which implies that the particle velocity vanishes in the normal direction $\mathbf{n}$,

$$\mathbf{n} \cdot \nabla\phi = 0. \quad (9)$$

The governing Eqs. (1) and (7) together with the relevant boundary conditions of the incident wave and the acoustically rigid walls are solved by using COMSOL MULTIPHYSICS. If the MPP is assumed to be rigid, Eq. (7) is excluded in solving the finite element model. The normal incidence absorption coefficient of the MPP absorber array is formulated as

$$\alpha = \frac{\rho_0 c_0 \int_0^h \mathrm{Re}[p*(y)u(y)]\mathrm{d}y}{|p_{in}|^2 h}, \quad (10)$$

where the asterisk represents the complex conjugate and Re is the real part of complex number.

III. NUMERICAL RESULTS AND DISCUSSION

The study conducted by Wang and Huang (2011) showed that a good absorption performance can be achieved by a MPP absorber array with three sub-cavities as shown in Fig. 1 based on the empirical impedance model given by Maa (1998) as formulated in Eq. (6) for the linear case. In their study, the effect of the local nonlinear feature of the perforations induced at moderate sound pressure on the absorption performance of the MPP absorber array was not considered. However, Ingard and Ising (1967) found that the acoustic impedance of an orifice would change with the incidence pressure at moderate sound pressure levels. Figure 2 shows variations of acoustic absorption of a single MPP absorber with cavity depth $D = 100$ mm measured experimentally under different acoustic incidence pressure. The experimental setup is described in Sec. IV. The parameters of the MPP is $t = 0.4$ mm, $d = 1$ mm, and $b = 6.36$ mm. The experimental results at five frequencies $f = 500$ Hz ($\bigcirc$), 700 Hz ($\times$), 800 Hz ($\square$), 900 Hz ($\triangle$), and 1100 Hz ($+$) is shown in Fig. 2. It is observed that the acoustic absorption increases with the incidence sound pressure level, which agrees with the observation given by Ingard and Ising (1967). The obvious change of absorption coefficient, acoustic resistance and reactance is observed at SPL around 100 dB. More than 10% increments of absorption are observed at SPL larger than 100 dB by comparing with the results measured at SPL around 76 dB. Figure 3 illustrates
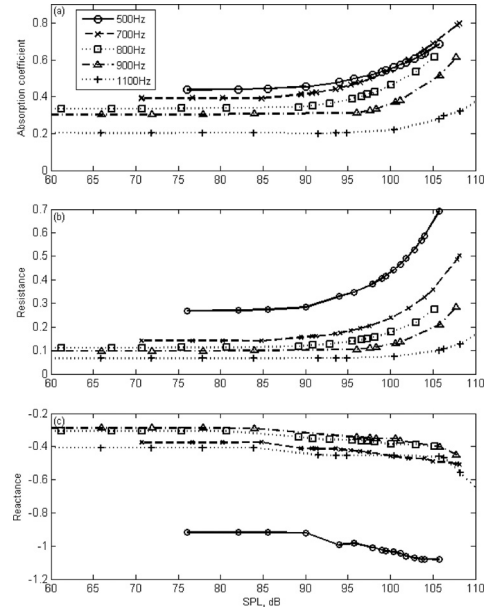

FIG. 2. Acoustic properties of MPP absorber with $t = 0.4$ mm, $d = 1$ mm, $b = 6.36$ mm, and $D = 100$ mm at different incidence sound pressure level. (a) Acoustic absorption; (b) acoustic resistance; (c) acoustic reactance.

the experimental normal incidence absorption coefficient of the single MPP absorber under different acoustic excitation, i.e., SPL = 90 dB ($\bigcirc$), 100 dB ($\times$), and 105 dB ($\square$). The maximum absorption coefficient is achieved at around 600 Hz due to the local resonance. An enhanced absorption coefficient can be noticed with the increase of the incident sound pressure level. The experimental results of the acoustic absorption as shown in Figs. 2 and 3 imply that the linear acoustic impedance is no longer valid at SPL around 100 dB due to the significant local nonlinearity effect of the perforations. Therefore, the present study aims to investigate the effect of the local nonlinearity of orifice on the acoustic behavior of the MPP absorber array at moderate sound intensity with the configuration as shown in Fig. 1. The duct height is $h = 99$ mm, and the widths of each sub-cavities are the same, i.e., $h/3$. The default cavity depths of the triple MPP absorber array are given as $D_1 = 50$ mm, $D_2 = 100$ mm, and $D_3 = 25$ mm. The codes are established for four types of MPPs with different thickness, orifice diameter, and perforation ratio, as listed in Table I, in order to explain the effect
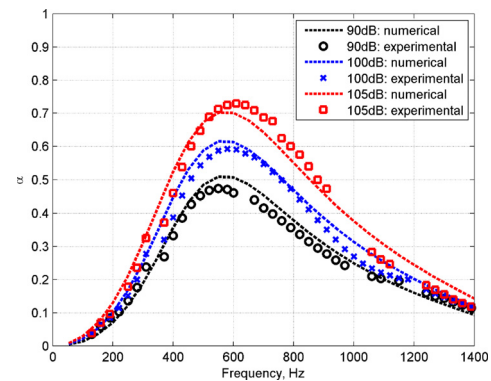

FIG. 3. (Color online) Absorption coefficient of single MPP absorber at different incidence sound pressure levels.

J. Acoust. Soc. Am. **143** (1), January 2018

Y. K. Chiang and Y. S. Choy   541

TABLE I. Parameters of MPPs used in the numerical investigations.

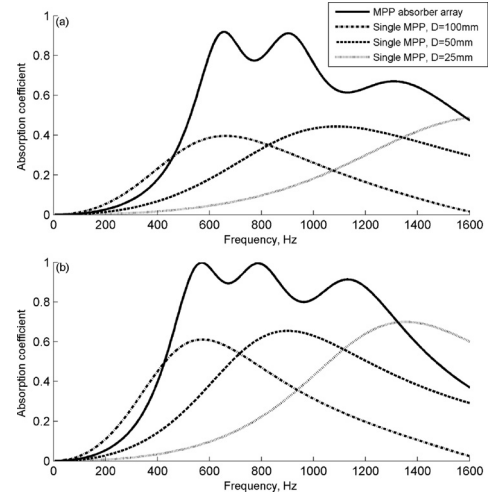|	Thickness, t	Orifice diameter, d	Perforation ratio, σ
MPP A	0.7 mm	1.2 mm	2.8%
MPP B	1 mm	1 mm	1.5%
MPP C	1 mm	1 mm	5.5%
MPP D	1 mm	1 mm	3.3%

FIG. 4. Comparison of the normal incidence absorption coefficients between the single MPP absorber and the MPP absorber array at the nonlinear regime, SPL = 110 dB. (a) MPP C with $\sigma = 5.5\%$; (b) MPP D with $\sigma = 3.3\%$. Other parameters: $d = t = 1$ mm. (—) MPP absorber array; (– · –) single MPP absorber with $D = 100$ mm; (– – –) single MPP absorber with $D = 50$ mm; (- - -) single MPP absorber with $D = 25$ mm.

of the local nonlinearity of orifice on the absorption performance of the MPP absorber array. The improvement of the absorption performance of the MPP absorber array by comparing with the single MPP absorber in the nonlinear regime is described in Sec. III A with the use of MPPs C and D which are of large orifice diameter $d = 1$ mm. The changes of the absorption behavior of the MPP absorber array between the linear and nonlinear regimes are explained with MPPs A and B in Sec. III B. In Sec. III C, the effect of the orifice local nonlinearity on the absorption mechanism of the MPP absorbers is discussed with MPP A. Moreover, the effect of the structural vibration on the absorption performance of MPP absorbers with the local nonlinearity of orifice is studied in Sec. III D with MPP A. The absorption performance of the MPP absorber array is described by the absorption coefficient α and the half-absorption bandwidth, which is the ratio of the upper limit frequency f_U and the lower limit frequency f_L for $\alpha > 0.5$, i.e., f_U/f_L. The acoustic behavior of the MPP absorber array due to the structural vibration of the perforated panel is described in Sec. III D. The numerical model is discretized as the triangular quadratic-Lagrange elements. For the model without vibration, the maximum element size is 0.005 m and the mesh consists of 3065 elements totally. For the model with structural vibration, the maximum element size is 0.003 m, and the mesh consists of 6044 elements and 33 elements for the acoustic and structural domains, respectively. The element size to the shortest wavelength ratio for the model without and with structural vibration are 0.025 and 0.015, respectively.

A. Comparison of sound absorption performance between the single MPP absorber and triple MPP absorber array in the nonlinear regime

Figure 4 compares the absorption coefficients of the triple MPP absorber array (solid line) with the single MPP absorber with cavity depths $D = 100$, 50, and 25 mm which are denoted by the dash-dot, dashed, and dotted lines, respectively. The incident sound pressure level is 110 dB. Figure 4(a) shows the sound absorption curves for MPP C. The poor absorption performance is observed for the single MPP absorbers, where the absorption coefficients are less than 0.5, due to the insufficient acoustic resistance provided by the large orifices with diameter $d = 1$ mm. In contrast, for the MPP absorber array, the overall sound absorption coefficients are relatively higher than those of single MPP absorbers. Based on the parallel absorption mechanism, three spectral peaks with $\alpha_{1,2,3} = 0.92$, 0.91, and 0.67 induced by the local resonance effects of sub-cavities are identified. Also, the half-absorption bandwidth is improved to 2.96. In

this regard, the MPP absorber array can provide better absorption performance with lower requirement of acoustic resistance. The absorption coefficients of three peaks can be further improved by reducing the number of orifices as shown in Fig. 4(b). Referring to Eq. (6a), such increment of absorption is attributed to the increase of acoustic resistance. Moreover, with the decrease of perforation ratio, the frequency range for half-absorption is shifted to lower frequencies due to the increase of acoustic reactance. Thus, the enhanced absorption performance of the MPP absorber array for a lower frequency range can be achieved by the MPP absorber array with smaller perforation ratio.

At moderate sound pressure, the acoustic response of the MPP absorber array changes with different acoustic pressure excitation. Figures 5(1a) to 5(3a) show the absorption performance of the MPP absorber array (solid line) for MPP D at incident pressure level 100, 110, and 120 dB, respectively. Three spectral peaks at $f_{1,2,3} = 570$, 785, and 1130 Hz can be observed in Fig. 5(2a). The absorption coefficients at three peaks achieved by the MPP absorber array are relatively higher than that contributed by the single MPP absorber with cavity depths $D = 100$ mm (dash-dot line), 50 mm (dashed line), and 25 mm (dotted line). Similar observations can be found in Fig. 5(3a) at 120 dB since the parallel absorption mechanism works in these two cases. Compared with the MPP absorber array at 100 dB, a noticeable increase of the absorption at the third peak is observed with the increase of incident sound pressure level. Also, the half-absorption bandwidth of the MPP absorber array is increased by about 35.7% from 3.08 to 4.18 when the incident sound pressure level increases from 100 to 120 dB due to the increase of acoustic resistance. Figures 5(1b) to 5(3b) illustrate the normal particle velocities over the MPP surface of the MPP absorber array at $f_1 = 570$ Hz (dash-dot line), $f_2 = 785$ Hz (dashed line), and $f_3 = 1130$ Hz (dotted line) for different sound pressure level. The magnitude of the velocity
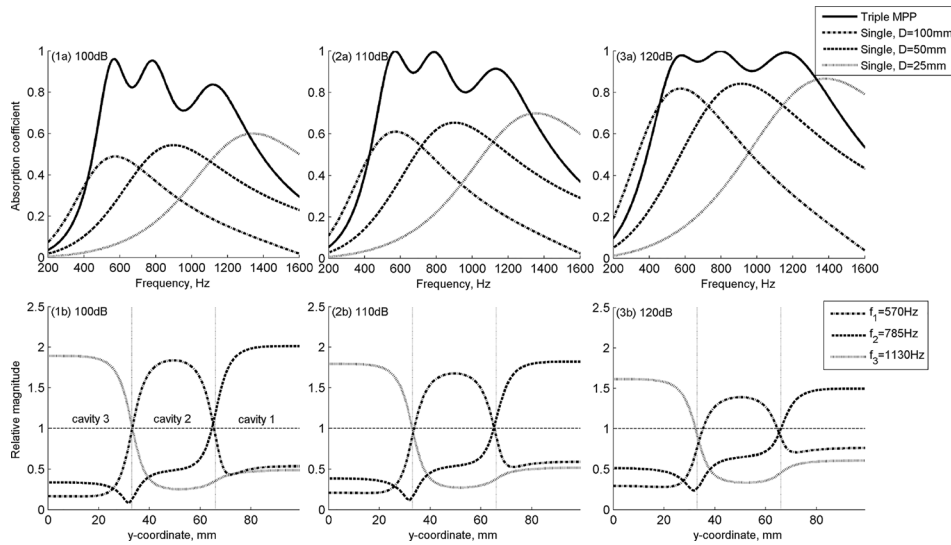
Y. K. Chiang and Y. S. Choy

FIG. 5. Comparison of the acoustic responses of the MPP absorber array in the nonlinear regime at different incidence sound pressure level. The results are obtained from MPP D. The subfigures in the first row show the normal absorption coefficients of the single MPP absorber and the MPP absorber array. The second row is the magnitude of particle velocities of the MPP absorber array over the MPP surface at $f_1 = 570\,\text{Hz}$ (dash-dot line), $f_2 = 785\,\text{Hz}$ (dashed line), and $f_3 = 1130\,\text{Hz}$ (dotted line). The magnitude is normalized by the particle velocity of the single MPP absorber.

is normalized by the particle velocity of the corresponding single MPP absorber. At 110 and 120 dB, the particle velocities over the whole resonating MPP absorber component are much higher than that of the single MPP absorber. For both cases, the magnitude of the particle velocity of the MPP absorber array over the resonating sub-cavities is higher than that of the single MPP absorber. As shown in Fig. 5(2b), the magnitude of the particle velocity over cavity 1 for f = 785 Hz (dashed line) is around 1.8 times larger than that in the single MPP absorber at 110 dB.

B. Comparison of sound absorption behaviors of MPP absorber array between linear and nonlinear regimes

Figure 6 shows the comparison of the normal incidence absorption coefficients of the triple MPP absorber array between the linear and nonlinear regimes. The sound pressure level is set to be 120 dB. The numerical results for the linear case are plotted in dashed lines. The solid curves represent the predicted absorption coefficients of the MPP absorber array with the effect of local nonlinearity of orifice at moderate sound excitation. Figure 6(a) illustrates the predicted results of MPP A. In the linear regime, three spectral peaks are found at $f_{1,2,3} = 555$, 760, and 1090 Hz which are associated with the local resonances of the three sub-cavities, respectively. The corresponding normal absorption coefficients at three peaks are $\alpha_{1,2,3} = 0.87$, 0.87, and 0.75, respectively. High absorption coefficients, i.e., $\alpha > 0.9$, cannot be achieved since the acoustic resistance of the MPP absorber array for MPP A with large orifice diameter is insufficient, i.e., $Z_{resist\ 1,2,3} = 0.12$, 0.13, and 0.16. When the MPP absorber array with the same parameters is subjected to moderate acoustic intensity, higher acoustic resistances are obtained, from Eq. (6a), due to the jet formation at the exit of the orifice. Hence, the whole absorption curve is improved to a higher level and also a broader bandwidth for $\alpha > 0.5$ is achieved when compared with the linear result. The corresponding absorption coefficients at $f_{1,2,3}$ are improved to $\alpha_{1,2,3} = 0.95$, 0.98, and 0.99 in the nonlinear regime. Moreover, noticeable frequency shifts are observed at moderate sound pressure level. Because of the jet formation at

the exit of the orifice, some air molecules are blown away, and hence the mass reactance due to the piston sound radiation at the tube end is reduced such that there is an improvement of acoustics impedance matching with ambient air at higher frequencies. Therefore, the local resonances of each sub-cavities are shifted to higher frequencies.

The predicted absorption coefficient of MPP B is shown in Fig. 6(b). As indicated by the dashed line, almost complete sound absorption is achieved at three resonance frequencies since the impedance matching condition is achieved for the linear case. However, there are two noticeable troughs in between the resonance frequencies on the absorption curve are found. These two absorption reductions are associated with the transition of the local-resonating sub-cavities. As a result, a wide bandwidth of high absorption cannot be maintained. On the other hand, at moderate sound pressure, the absorption curve is smoothed out without significant resonance peak, and the absorption performance of the MPP absorber array is maintained at $\alpha > 0.8$ from $f = 415$ to $1090\,\text{Hz}$. The disappearance of the absorption
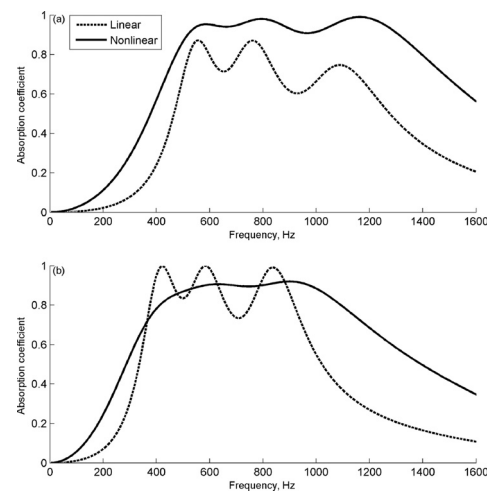

FIG. 6. Comparison of the normal incidence absorption coefficients of the MPP absorber array between the linear and nonlinear regimes. (a) MPP A with $d = 0.7\,\text{mm}$, $t = 1.2\,\text{mm}$, and $\sigma = 2.8\%$; (b) MPP B with $d = t = 1\,\text{mm}$ and $\sigma = 1.5\%$. The depths of sub-cavities are $D_1 = 50\,\text{mm}$, $D_2 = 100\,\text{mm}$, and $D_3 = 25\,\text{mm}$.
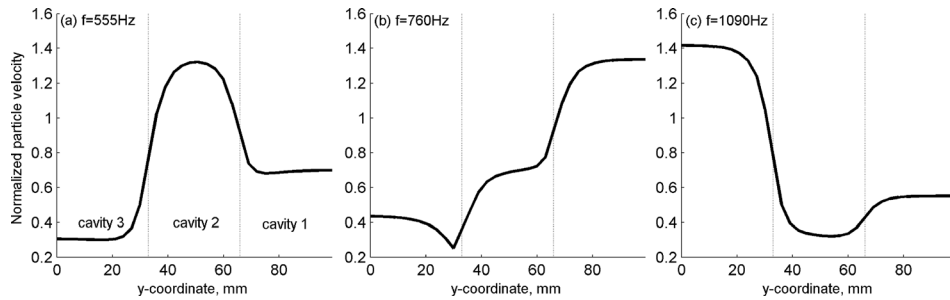
FIG. 7. The normal particle velocity over the surface of MPP A. The magnitude is normalized by the particle velocity of incidence wave at 120 dB. (a) $f = 555$ Hz; (b) $f = 760$ Hz; (c) $f = 1090$ Hz.

peaks indicates that the local resonance effects of each sub-cavity are reduced because of the possible different absorption mechanisms between the linear and nonlinear regimes, which will be discussed in Sec. III C.

The particle velocity over the surface of MPP A triple absorber array normalized by the particle velocity of incident wave at 120 dB for three local resonance frequencies are shown as Figs. 7(a)–7(c). It is observed that the particle velocity over the resonating MPP components is higher than that of the incident wave. The particle velocities over the resonating MPP surface are around 1.32, 1.33, and 1.41 times higher than that of the incident wave for $f_{1,2,3} = 555$, 760, and 1090 Hz, respectively. Due to the high particle velocity induced by the acoustic excitation, the nonlinear term of the acoustic resistance in Eq. (6a) would be comparatively higher than the linear term. The ratios of the nonlinear term of resistance to the linear term over the corresponding resonating sub-cavities can reach 4.9, 3.43, and 2.8 at $f_{1,2,3} = 555$, 760, and 1090 Hz, respectively, which implies that the local orifice nonlinearity effect on the acoustic response of the MPP absorber array would be significant. As such, the orifice nonlinearity is necessary to be considered in this moderate incident sound pressure level.

Figure 8 depicts the normal particle velocity on the surface of MPP A absorber array at the local resonance frequencies $f_{1,2,3} = 555$, 760, and 1090 Hz. The magnitudes of the particle velocity are normalized by normal particle velocity of the single MPP A absorber at the same frequencies $f_{1,2,3}$ with the cavity depths $D = 100$, 50, and 25 mm, respectively, in the linear regime, i.e., at 90 dB. At the lowest resonance frequency $f_1 = 555$ Hz, as shown in Fig. 8(a), the normalized particle velocity over cavity 2 is relatively higher than that of cavity 1 and cavity 3 for both linear (dashed line) and nonlinear regimes (solid line) due to the strong local resonance. Although the curves of the particle velocity over the MPP for the linear and nonlinear cases are similar, the magnitude corresponding to the MPP absorber array subjected to

moderate sound pressure is significantly higher than the linear one. Similar observation can be made for the second and third resonance frequencies as illustrated by Figs. 8(b) and 8(c), respectively. The absorption peaks at $f_2 = 760$ Hz and $f_3 = 1090$ Hz, found in Fig. 6(a), are achieved due to the local resonances occur in cavity 1 and cavity 3, respectively. As shown in Fig. 8(b), for the linear case, the particle velocity over cavity 1 at $f_2 = 760$ Hz is about 2 times larger than that of the single MPP absorber. The magnitude of the normalized particle velocity is further increased to about 33 in the nonlinear regime. For the MPP A absorber array, the sub-cavities can be excited to resonance in both linear and nonlinear regimes. At moderate sound pressure, the high particle velocity is induced in the orifices. The acoustic resistance increases with the particle velocity, and thus more sound energy can be dissipated in the resonating cavity. As a result, the effect of the local resonance on the acoustic absorption is enhanced in the nonlinear regime.

C. Effect of the orifice local nonlinearity on the absorption mechanism of the MPP absorbers

The comparison of the normal incidence absorption coefficient of the MPP absorbers for MPP A between the linear and nonlinear regimes is illustrated in Fig. 9. The numerical result for the linear case is plotted in solid line. The predicted absorption coefficients of the MPP absorber array at moderate sound excitation SPL = 100, 110, and 120 dB are represented by the dashed, dotted, dash-dot lines, respectively. Figure 9(a) demonstrates the effect of the incidence pressure amplitude on the acoustic absorption of the single MPP absorber. It is found that the absorption coefficient and the half-absorption bandwidth increase with the incidence sound pressure level. The peak absorption coefficient can reach to 0.87 for MPP A at SPL = 120 dB, which is 2.35 times higher than that of the linear case. The similar observation can be obtained for the triple MPP absorber array as
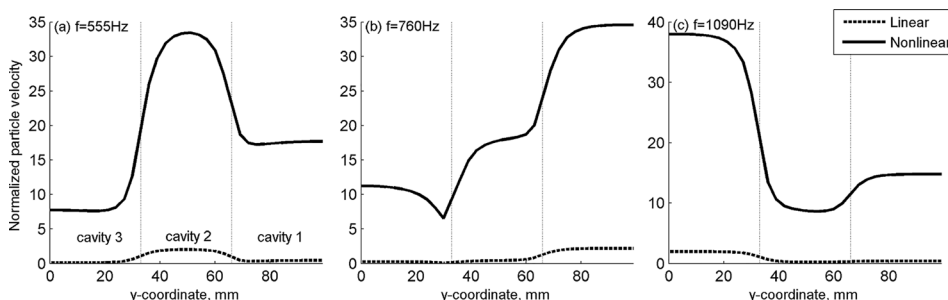

FIG. 8. The normal particle velocity over the surface of MPP A. The magnitude is normalized by the particle velocity in the corresponding single MPP absorber in the linear regime at 90 dB. (a) $f = 555$ Hz; (b) $f = 760$ Hz; (c) $f = 1090$ Hz.
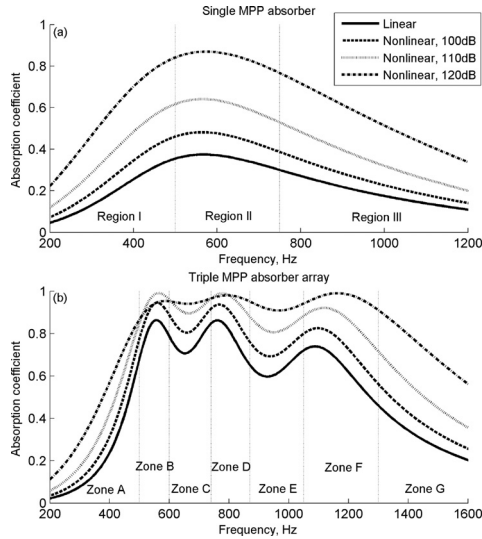
FIG. 9. Comparison of the normal incidence absorption coefficients of MPP A between the linear and nonlinear regimes. (a) Single MPP absorber; (b) triple MPP absorber array. (—) Linear; (– – –) 100 dB; (- - -) 110 dB; (– · –) 120 dB.
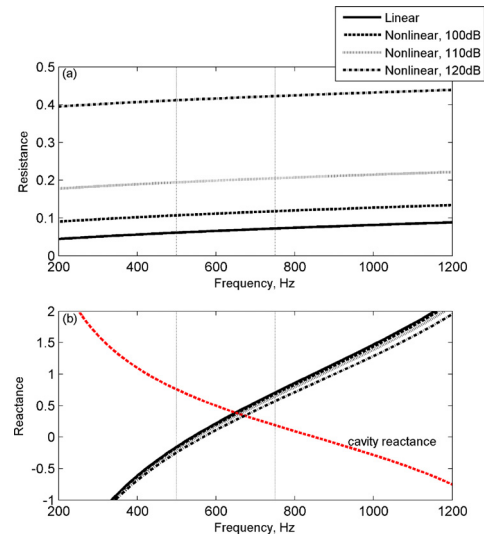

FIG. 10. (Color online) Normalized surface impedance of the single MPP absorber for MPP A. (a) Specific acoustic resistance; (b) specific acoustic reactance. (—) Linear; (– – –) SPL = 100 dB; (- - -) SPL = 110 dB; (– · –) SPL = 120 dB.

shown in Fig. 9(b). In the linear regime, based on the parallel absorption mechanism, three spectral peaks are found at $f_{1,2,3} = 555$, 760, and 1090 Hz which are associated with the local resonances of the three sub-cavities $D_2 = 100$ mm, $D_1 = 50$ mm, and $D_3 = 25$ mm, respectively. The corresponding normal absorption coefficients at three peaks are $\alpha_{1,2,3} = 0.87$, 0.87, and 0.75, respectively. When the MPP absorber array with the same parameters is subject to moderate acoustic intensity, the amplitude of the whole absorption spectrum increases and also a broader bandwidth for $\alpha > 0.5$ is achieved when compared with the linear result. The corresponding absorption coefficients at $f_{1,2,3}$ are improved to $\alpha_{1,2,3} = 0.99$, 0.99, and 0.92 in the nonlinear regime at 110 dB, respectively. When the incidence pressure level further increases to SPL = 120 dB, the first spectral peak at 580 Hz is reduced to $\alpha_1 = 0.95$. The smoothed absorption performance of the MPP absorber array at moderate intensity sound is induced by the added-mass effect from the neighboring sub-cavity. The explanation would be described in detail with Figs. 10 and 11.

The absorption mechanism for the simple configuration with single backing cavity can be explained by dividing the acoustic response into three regions: *region I* is at low frequency range with stiffness effect; *region II* is the resonating part; *region III* is at high frequency range with mass effect. In region I, it is the zone of acoustic reactance mismatch since the stiffness effect of the backing cavity is domain as shown in Fig. 10(b) and hence the resultant reactance of the MPP absorber is negative. For both linear and nonlinear cases, the absorption coefficient is unable to reach a high value due to the reactance mismatch. However, comparing the results between the linear regime and that at SPL = 120 dB, the absorption performance of the single MPP absorber is comparatively better at moderate sound pressure level. In the nonlinear regime, the vortex ring formed at the exit of the perforations, which induces a higher acoustic resistance on the MPP as shown in Fig. 10(a), and

hence improves the absorption performance of the MPP absorber. For region II, the stiffness effect of the backing cavity is balanced by the virtual mass effect of the MPP. In this frequency range, the MPP absorber performs the best when compared with the absorption performance in regions I and III since the MPP absorber is resonating and hence more acoustic energy can be dissipated in this frequency range. The absorption performance of MPP absorber is also better under moderate acoustic excitation since the acoustic resistance of the MPP at SPL = 120 dB is 0.415, which is 6.48 times higher that than in the linear regime at 570 Hz with maximum absorption coefficient. At higher frequency, it is regarded as region III, where the virtual mass effect of the MPP is dominant. The relatively higher absorption coefficient is also achieved for the nonlinear case due to the acoustic resistance is higher which bring benefit to sound dissipation. Therefore, the absorption performance of the single MPP absorber is improved at moderate intensity sound due to the larger acoustic resistance for both regions.
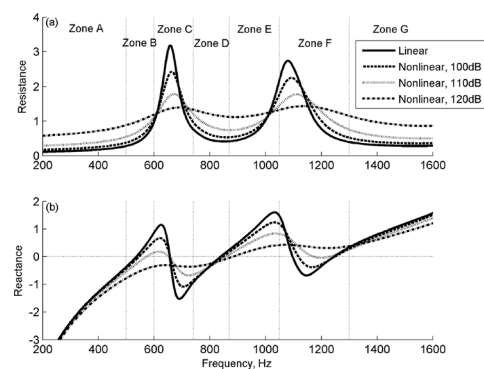

FIG. 11. Normalized surface impedance of the parallel-arranged MPP absorber array for MPP A. (a) Specific acoustic resistance; (b) specific acoustic reactance. (—) Linear; (– – –) SPL = 100 dB; (- - -) SPL = 110 dB; (– · –) SPL = 120 dB.

J. Acoust. Soc. Am. **143** (1), January 2018

Y. K. Chiang and Y. S. Choy   545

The absorption mechanism of the parallel-arranged MPP absorber array is more complicated than that of the single MPP absorber. The acoustic behavior of the triple MPP absorber array can be divided into seven zones: zone A is at low frequency range with stiffness effect; zones B, D, and F are the first, second, and third resonating frequency ranges; zones C and E are the transition stages; zone G is at high frequency range with mass effect. As shown in Fig. 9(b), first, it is observed that the absorption performance of the MPP absorber array is better than that in the linear regime. Second, the insufficient sound absorption at the trough point at $f = 650$ and 930 Hz for the linear case is improved with the increase of acoustic excitation. The first observation can be explained by the idea stated for the single MPP absorber since the acoustic responses of the MPP absorber array in zones A and G are the same as that of regions I and III of the single MPP absorber, respectively. Three spectral peaks are found at $f_{1,2,3} = 555$, 760, and 1090 Hz due to the local resonance occurs at zones B, D, and F, respectively. For the second observation, the improvement of the absorption coefficient at troughs with the incidence pressure level can be explained by the total acoustic impedance of the MPP absorber array obtained by using the electro-acoustic circuit model (Yairi and Sakagami, 2011). According to the electro-acoustic circuit model, the equivalent acoustic impedance of the multiple absorber array can be formulated as

$$Z_{total} = \left[\sum_{j=1}^{N} \frac{1}{N} \times \frac{1}{Z_j} \right]^{-1},$$

where Z_j is the specific acoustic impedance of the jth MPP absorber component, where $j = 1, \ldots, N$ and N is the number of MPP absorber component. In the current study, triple MPP absorber array is considered, hence $N = 3$. The acoustic impedance of the MPP absorber array for MPP A is shown as Fig. 11. In the transition stage, i.e., zones C, at frequency around 630 Hz, the acoustic reactance of the MPP absorber array in the linear regime is high due to the virtual mass effect of the MPP absorber component with $D_2 = 100$ mm. The ability of the MPP absorber array to dissipate sound energy is degraded due to the reactance mismatch as shown in Fig. 11(b). However, at moderate acoustic excitation, a negative mass effect is induced since part of the attached mass in the orifice is blown away by the jet. Therefore, the acoustic reactance of the MPP is reduced such that there is higher acoustics impedance matching with ambient air, which allows the sound wave to penetrate the absorber to be dissipated. On the other hand, at frequency around 700 Hz, an increasing acoustic reactance can be found with the increase of incidence pressure. Zone C is the transition stage that the resonating component is changed from cavity 2 to cavity 1. The acoustic energy would be dissipated in both cavity 1 and 2. With the increase of sound pressure level, the situation of reactance mismatch of MPP absorber component with $D_2 = 100$ mm is improved and thus more acoustic energy would propagate to cavity 2 when compared with the linear case. The contribution of the neighboring cavity provides an added mass effect to the overall reactance of the
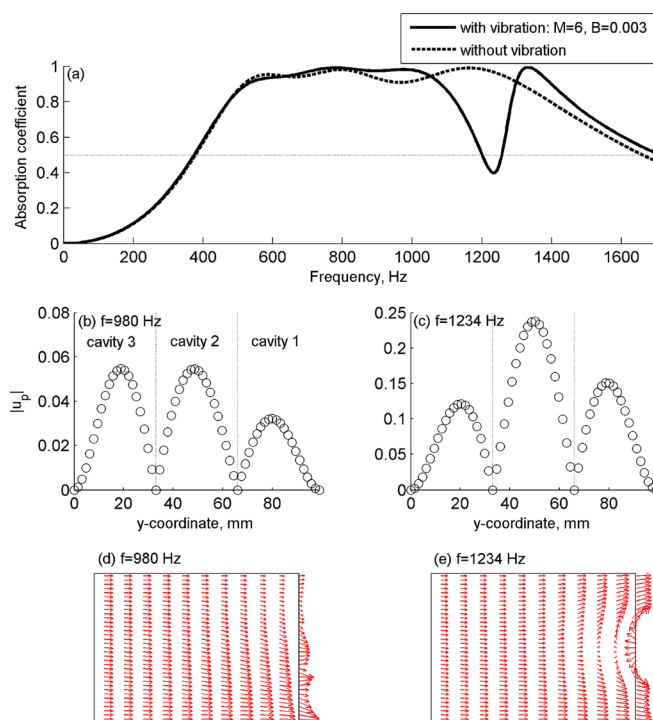

FIG. 12. (Color online) Comparison of the acoustic responses of the MPP absorber array between flexible and rigid MPP in the nonlinear regime. The results are obtained from MPP A. (a) Normal incidence absorption coefficients; (b) and (c) amplitude of the panel vibrating velocities; (d) and (e) the acoustic intensity vector in the duct.

MPP absorber array in the nonlinear regime. As a result, the absorption performance at the trough is improved at moderate sound intensity since the effect of the reactance mismatch is reduced due to the added-mass effect given by the neighboring sub-cavity. The similar observation around 1000 Hz can be obtained for the second trough at zone E.

D. Effect of the structural vibration on the absorption performance of MPP absorbers with the local nonlinearity of orifice

Generally, the micro-perforated panel can be made of any material. When a light weight MPP is used under moderate acoustic excitation, say 120 dB, the effect of the structural vibration on the acoustic absorption of the MPP absorber array would not be ignored. Figure 12(a) compares the normal incidence absorption coefficients between the rigid MPP (dashed line) and the flexible MPP with vibration (solid line). The numerical results are predicted for MPP A with dimensionless surface density $M = 6$ and bending stiffness $B = 0.003$, which have been normalized by $\rho_0 h$ and $\rho_0 c_0^2 h^3$, respectively. In this study, the MPP is clamped to the backing cavity at $y = 0$ and h, and simply supported by two partitions. The absorption coefficient of the MPP absorber array remains at high level ($\alpha > 0.8$) for the low frequency range until $f = 1000$ Hz. However, the absorption performance drops dramatically at around the third peak due to the effect of structural vibration. The trough observed at $f = 1234$ Hz leads to the half-absorption bandwidth reduction, i.e., half-absorption bandwidth $= f_U/f_L$, which decreases from 4.38 to 3.19. The magnitude of the panel velocity in x-

direction at $f = 980$ and 1234 Hz is presented in Figs. 12(b) and 12(c). At $f = 980$ Hz, the perforated panel is excited with the surface velocity, i.e., $u_p < 0.06$ m/s. As shown in Fig. 12(d), the acoustic energy is attracted to both sub-cavities for sound absorption since the effect of the structural vibration is insignificant at this frequency. Hence, the absorption performance can be maintained. However, at $f = 1234$ Hz, which is the local resonance frequency of cavity 3 roughly, the MPP vibrates vigorously especially for the middle region of the MPP due to the structural resonance. The maximum velocity of the panel vibration is $u_p = 0.238$ m/s at $f = 1234$ Hz, which is four times larger than that at $f = 980$ Hz. As indicated by the acoustic intensity vector inside the duct in Fig. 12(e), the strong structural vibration in the middle region of the MPP would cause the sound reflection. As a result, the acoustic performance of the MPP absorber array is degraded since the middle component MPP absorber fails to absorb sound energy.

As shown in Fig. 12, the absorption performance of the MPP absorber array would be greatly affected by the structural vibration of the perforated panel. The material properties of the MPP should be selected appropriately in order to obtain the optimal absorption performance with desirable bandwidth when it is subjected to moderate sound pressure. Figure 13(a) shows the optimal results with respect to the half-absorption bandwidth of the single MPP absorber of $D = 100$ mm (dashed line) and triple MPP absorber array (dash-dot line) for MPP A with vibration at 120 dB incident pressure level. Figures 13(b) and 13(c) display the half-absorption bandwidth contour as a function of mass ratio M and bending stiffness B for the single MPP absorber and triple MPP absorber array, respectively. The solid lines on the contour show the peak value of the absorption coefficient achieved by MPP absorbers for the corresponding M and B.

For the flexible single MPP absorber with optimal parameters $M = 26$ and $B = 0.008$, an absorption peak is induced by the structural resonance at a higher frequency $f = 1108$ Hz. As shown by Lee *et al.* (2005), such high absorption is caused by the high relative velocities between the panel and air particles. However, by comparing the result of rigid MPP represented by the solid line in Fig. 13(a), the low frequency absorption performance of the optimal panel is degraded due to the effect of the structural vibration found at $f = 212$ Hz such that the half-absorption bandwidth is reduced from 3.21 to 2.99. For the triple MPP absorber array with $M = 20$ and $B = 0.002$, the absorption pattern are different between the cases with and without the panel vibration effect, which are represented by the dotted and dash-dot lines, respectively. However, it shows that the negative effect caused by the structural vibration of the panel on the half-absorption absorption of the MPP absorber array is significantly less than that of the single MPP absorber. Moreover, compared to the single MPP absorber, the contours show that the requirement of the bending stiffness of the optimal triple MPP absorber array can drop from 0.008 to 0.002 by 75% in order to achieve a wide half-absorption bandwidth. The corresponding optimized bandwidth of the MPP absorber array can reach to 4.47 which significantly increase by about 49% when comparing with the single MPP absorber.

IV. EXPERIMENTAL VALIDATION

In order to validate the numerical results, the normal incidence absorption coefficients of the MPP absorber array were measured experimentally in both linear and nonlinear regimes by using the two-microphone method. The experimental setup is illustrated in Fig. 14. The incident sound is generated by a loudspeaker. A digital-to-analogue conversion card (PCI-M10-16 E-1 from National Instruments) was used to general the signal which is amplified by a B&K's amplifier (Lab Gruppen 300). One pair of 1/2 in. microphones (B&K type 4947) were used and connected to a B&K's Nexus conditioning amplifier type 2693. The signals from the microphones were digitized by the National Instruments card PCI-4452. The A/D and D/A processes were both controlled by National Instruments' LABVIEW program. The rectangular MPP with parameters $t = 0.4$ mm, $d = 0.65$ mm, and $\sigma = 1.76\%$ was made of stainless steel with density $\rho = 8060$ kg/m^3 and Young's modulus $E = 200$ GPa. The backing cavities were partitioned by two aluminum plates with thickness 1 mm. The
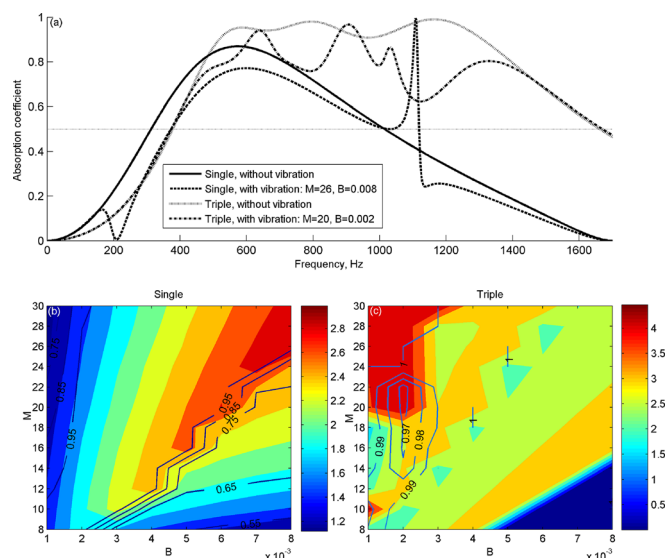

FIG. 13. (Color online) Optimal spectrum with respect to the half-absorption bandwidth for the single MPP absorber and MPP absorber array in the nonlinear regime. The top figure is the normal absorption coefficients at optimal mass ratio and bending stiffness. The subfigures below show the optimal half-absorption bandwidth contour as a function of mass ratio M and bending stiffness B. (b) Single MPP absorber; (c) triple MPP absorber array.
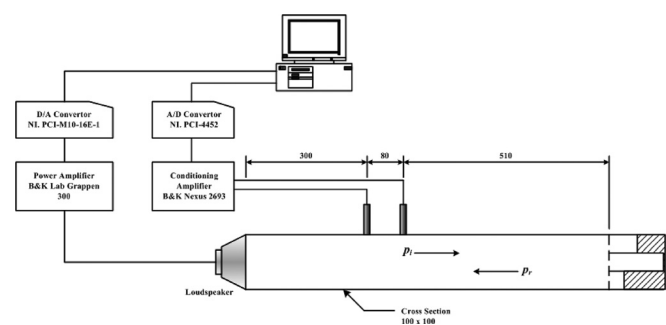

FIG. 14. Experimental setup for measuring the normal incidence absorption coefficient by using the two-microphone transfer-function method.

J. Acoust. Soc. Am. **143** (1), January 2018
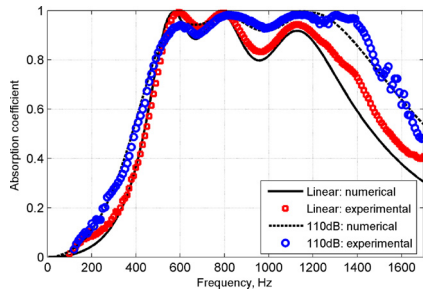
Y. K. Chiang and Y. S. Choy   547

FIG. 15. (Color online) Comparison between the numerical prediction and the experimental results of the MPP absorber array. (—) Numerical result in linear regime; (– – –) numerical result at SPL = 110 dB; (□) experimental result in linear regime; (○) experimental result at SPL = 110 dB.

depths of three sub-cavities were $D_1 = 50$ mm, $D_2 = 99$ mm, and $D_3 = 25$ mm. The duct walls and cavity walls were made of acrylic of thickness 15 mm. The cross-section area of the rectangular duct was 100 mm × 100 mm. The first cut-on frequency is around 1700 Hz. The absorption performance of the MPP absorber array was measured at 110 dB.

The comparison of normal incidence absorption coefficients between the numerical predictions (solid line) and the experimentally measurements (open circle) for the prototype MPP absorber array without vibration in the linear and nonlinear regimes is shown in Fig. 15. Three spectral peaks are observed from the measurement and matched with the predictions observed in both linear and nonlinear cases. There is a good agreement between the numerical and measured results for the resonance frequencies and the sound absorption levels. The maximum relatively error is found as 10.3% at $f = 1400$ Hz. The relative errors for three spectral peaks are 0.76%, 0.46%, and 1.34% at $f = 600$, 810, and 1190 Hz, respectively. Such error found at high frequency could be induced by two following possible reasons. (1) There is a structural damping in the system. (2) The diameters among the orifices of the MPP may be different due to the limitation of the manufacturing process. The absorption improvement with broader half-absorption bandwidth at moderate sound pressure, as mentioned in Sec. III A, is successfully achieved by the experiments. Comparing with the result in the linear regime, the half-absorption bandwidth of the MPP absorber array under moderate acoustic excitation is increased from 3.42 to 4.18. The experimental result of the MPP absorber array was only compared with the numerical result predicted by the finite element model without vibration for model validation in the present study. The effect of the structural vibration on the absorption performance of the MPP absorber array is small and can only be found experimentally if the MPP is made of a lighter material and subjected to a higher acoustic excitation.

V. CONCLUSIONS

The acoustic performance of the microperforated panel (MPP) absorber array subjected to moderate acoustic excitation is studied. A two-dimensional numerical model is established to investigate the acoustic behaviors of the MPP absorber array under normal incidence in the nonlinear

regime. The normal incidence absorption coefficients of the prototype MPP absorber array are measured experimentally in both linear and nonlinear regimes to validate the numerical simulation. The following conclusions are made.

(1) The acoustic behaviors of the MPP absorbers under moderate acoustic excitation are significantly different from that in the linear regime due to the effect of local nonlinearity of orifice. Starting at incident sound pressure level 100 dB, there is a significant variation on the acoustic impedance and absorption performance of the MPP absorber from frequency around 300 to 1100 Hz. At the incident sound pressure beyond 100 dB, more than 10% increments of absorption and acoustic resistance induced by the local nonlinearity of orifice are observed by comparing with the results measured in linear regime. The variation of the acoustic properties of MPP absorber indicates that the local nonlinearity effect of orifice exists under acoustic excitation around 100 dB, at which the acoustic field is linear.

(2) With appropriate structural and perforation property of MPP, the MPP absorber array in the non-linear regime has higher level and wider bandwidth of sound absorption than that in the linear regime under the moderate acoustic pressure excitation less than about 120 dB. This is caused by an improvement of equivalent acoustics impedance matching with ambient air over wide frequency range that is attributed to the negative mass effect by jet formation at the orifice in non-linear regime. The negative mass would reduce the acoustic impedance over the resonating sub-cavity at around the local-resonating frequencies and become added-mass effect on neighboring sub-cavities at the transition zone in between two local-resonating frequencies.

(3) When the sound pressure level is too high, the negative mass effect is too strong and it weakens the equivalent acoustics impedance match with ambient air. As a result, it diminishes the local resonance effects of the resonating component MPP absorber and lower sound absorption would be obtained at local-resonating frequencies.

(4) The absorption performance of the MPP absorber array would be degraded due to the effect of panel vibration. The vigorous vibration of the panel leads to sound reflection such that less acoustic energy can penetrate and be dissipated by the MPP absorber array. To avoid the performance degradation induced by panel vibration, the optimal structural properties of MPP absorber array was determined as M = 20, B = 0.002, $d = 1.2$ mm, $t = 0.7$ mm, and $\sigma = 2.8\%$, which can achieve half-absorption bandwidth 4.47 at moderate sound pressure level 120 dB.

(5) The finite element model of the MPP absorber array at moderate sound pressure is validated by experiment. The measured absorption coefficients of the MPP absorber array agree with the predicted results with a relative error of less than 10.5%. The half-absorption bandwidth of the MPP absorber array with $t = 0.4$ mm, $d = 0.65$ mm, and $\sigma = 1.76\%$ can reach 4.18 at SPL = 110 dB.

Y. K. Chiang and Y. S. Choy

Crocker, M. J. (**1998**). *Handbook of Acoustics* (Wiley, New York), pp. 203–210.

Cummings, A. (**1986**). "Transient and multiple frequency sound transmission through perforated plates at high amplitude," J. Acoust. Soc. Am. **79**, 942–951.

Cummings, A., and Eversman, W. (**1983**). "High amplitude acoustic transmission through duct terminations: Theory," J. Sound Vib. **91**, 503–518.

Hersh, A. S., Walker, B. E., and Celano, J. W. (**2003**). "Helmholtz resonator impedance model, Part 1: Nonlinear Behavior," AIAA J. **41**, 795–808.

Ingard, K. U. (**1994**). *Notes on Sound Absorption Technology* (Noise Control Foundation, Poughkeepsie, NY), Chap. 3, pp. 1–18.

Ingard, U., and Ising, H. (**1967**). "Acoustic nonlinearity of an orifice," J. Acoust. Soc. Am. **42**, 6–17.

Ingard, U., and Labate, S. (**1950**). "Acoustic circulation effects and the nonlinear impedance of orifices," J. Acoust. Soc. Am. **22**, 211–218.

Lee, D. H., and Kwon, Y. P. (**2004**). "Estimation of the absorption performance of multiple layer perforated panel systems by transfer matrix method," J. Sound Vib. **278**, 847–860.

Lee, Y. Y., Lee, E. W. M., and Ng, C. F. (**2005**). "Sound absorption of a finite flexible micro-perforated panel backed by an air cavity," J. Sound Vib. **287**, 227–243.

Maa, D. Y. (**1975**). "Theory and design of microperforated panel sound-absorbing constructions," Sci. Sin. **18**, 55–71, available at http://engine.scichina.com/publisher/scp/journal/Math%20A0/18/1/10.1360/ya1975-18-1-55?slug=full%20text.

Maa, D. Y. (**1996**). "Microperforated panel at high sound intensity," Acta Acust. **21**, 10–14, available at http://en.cnki.com.cn/Article_en/CJFDTOTAL-XIBA601.001.htm.

Maa, D. Y. (**1998**). "Potential of microperforated panel absorber," J. Acoust. Soc. Am. **104**, 2861–2866.

Mu, R. L., Toyoda, M., and Takahashi, D. (**2011**). "Sound insulation characteristics of multi-layer structures with a microperforated panel," Appl. Acoust. **72**, 849–855.

Park, S.-H. (**2013**). "A design method of micro-perforated panel absorber at high sound pressure environment in launcher fairings," J. Sound Vib. **332**, 521–535.

Sakagami, K., Morimoto, M., and Koike, W. (**2006**). "A numerical study of double-leaf microperforated panel absorbers," Appl. Acoust. **67**, 609–619.

Salikuddin, M., and Ahuja, K. K. (**1983**). "Acoustic power dissipation on radiation through duct terminations: Experiments," J. Sound Vib. **91**, 479–502.

Sivian, L. J. (**1935**). "Acoustic impedance of small orifices," J. Acoust. Soc. Am. **7**, 94–101.

Takahashi, D., and Tanaka, M. (**2002**). "Flexural vibration of perforated plates and porous elastic materials under acoustic loading," J. Acoust. Soc. Am. **112**, 1456–1464.

Tayong, R., Dupont, T., and Leclaire, P. (**2010**). "On the variations of acoustic absorption peak with particle velocity in micro-perforated panels at high level of excitation," J. Acoust. Soc. Am. **127**, 2875–2882.

Thurston, G. B., Jr., Hargrove, L. E., and Cook, B. D. (**1957**). "Nonlinear properties of circular orifices," J. Acoust. Soc. Am. **29**, 992–1001.

Wang, C., and Huang, L. (**2011**). "On the acoustic properties of parallel arrangement of multiple micro-perforated panel absorbers with different cavity depths," J. Acoust. Soc. Am. **130**, 208–218.

Wang, C., Huang, L., and Zhang, Y. (**2014**). "Oblique incidence sound absorption of parallel arrangement of multiple micro-perforated panel absorbers in a periodic pattern," J. Sound Vib. **333**, 6828–6842.

Wang, C. Q., and Choy, Y. S. (**2015**). "Investigation of a compound perforated panel absorber with backing cavities partially filled with polymer materials," J. Sound Vib. Acoust. **137**, 044501.

Wang, X. N., Choy, Y. S., and Cheng, L. (**2012**). "Hybrid noise control in a duct using a light micro-perforated plate," J. Acoust. Soc. Am. **132**, 3778–3787.

Yairi, M., and Sakagami, K. (**2011**). "Excess sound absorption at normal incidence by two microperforated panel absorbers with different impedance," Acoust. Sci. Technol. **32**, 194–200.

Zha, X., Kang, J., Zhang, T., Zhou, X., and Fuchs, H. (**1994**). "Application approach for microperforated panel sound absorbers," Acta Acust. **19**, 256–265, available at http://en.cnki.com.cn/Article_en/CJFDTOTAL-XIBA404.002.htm.

Zhang, Z. M., and Gu, X. T. (**1998**). "The theoretical and application study on a double layer microperforated sound absorption structure," J. Sound Vib. **215**, 399–405.